Initial Pointing Calibrations for the DSS 13 34-Meter Beam-Waveguide Antenna

L. S. Alvarez
Ground Antennas and Facilities Engineering Section

The beam pointing of the new DSS 13 beam-waveguide antenna at the Goldstone Venus site was calibrated during the postconstruction performance testing period from July 1990 through January 1991. The pointing calibrations were based on errors measured on radio sources at both the Cassegrain and centerline beam-waveguide focal points. The blind pointing performance goal of 5.0 mdeg, 3-sigma at Ka-band (32 GHz) was demonstrated to be met for low (<10 mph) wind conditions.

I. Introduction

This article describes the beam pointing for the new DSS 13 34-m beam-waveguide (BWG) antenna at the Goldstone Venus site from July 1990 through January 1991. An outline drawing of the DSS 13 antenna is shown in Fig. 1. During the calibration period, efficiency and pointing performance were characterized at X- and Ka-band frequencies (8450 MHz and 32 GHz, respectively) at both the f1 (Cassegrain) and f3 (centerline BWG) focal points illustrated in Fig. 1.

The objectives of the DSS 13 pointing calibrations were (1) to meet the specifications stated in the project Functional Requirements Document, and (2) to provide a systematic pointing-error model sufficient to carry out efficiency measurements. The beam-pointing accuracy required in less than 10-mph wind is 8 mdeg for X-band and 5 mdeg for Ka-band. These are 3-sigma blind-pointing specifications over the whole sky, with the pointing error defined to be the root sum square of the simultaneous errors sensed in the elevation and cross-elevation axes. It was decided that the 5-mdeg specification would be the goal for antenna pointing at both frequencies.

II. Pointing Calibration Overview

The primary objective of the antenna beam-pointing calibrations is to generate a pointing-error-correction model to be loaded into the antenna pointing system so that systematic pointing errors can be compensated for during tracking operations. The basic iterative procedure is to first measure pointing errors on a collection of radio sources adequately distributed over the sky. The negatives of the measured errors, termed corrections, are then fitted by the method of least squares to a set of pointing-error model terms. The resultant coefficients are loaded into the antenna control subsystem (ACS) computer, which then generates real-time pointing corrections as a function of antenna azimuth and elevation position. The process is repeated until suitable and predictable pointing perfor-

mance is attained. A detailed summary of the DSS 13 f1 and f3 pointing calibration methods employed and final results obtained are given below.

III. Beam-Pointing Measurements

A boresighting technique developed in 1989–1990 by R. L. Riggs of the Ground Antennas and Facilities Engineering Section was used to accurately point the antenna at the radio sources used in the calibration process. The method used was a "seven-point" boresight technique. This method moved the antenna sequentially along the cross-elevation (xel) and elevation (el) axes, both on and off the source. In each axis, the antenna was commanded to move off-source by 10 half-power (one-sided) beamwidths, one half-power beamwidth at the "3-dB" point, approximately 0.576 half-power beamwidths at the "1-dB" point, and on-source. Then, similar position offsets are executed for the other side. Noise-temperature measurements obtained at each offset are normalized with respect to a baseline generated by the off-source measurements.

The adjusted data points for a single axis are fit to a linearized exponential from which computed coefficients yield estimates of pointing error, half-power beamwidth, and peak temperature. Pointing measurements resulting from each axis scan are called scan errors. A pair of scans (one xel and one el) are considered to be one measurement point. The seven pointing offsets for each new scan are corrected for pointing errors found from the previous scans during the track. This is accomplished by centering those offsets about the running sum of the scan pointing corrections and then sending them as position offsets to the antenna via the ACS. The scan corrections are just the negatives of the scan errors. During the measurements, the principal outputs of the calibration software are an efficiency file and a pointing file. The efficiency file consists of time, azimuth, elevation, and xel and el estimates of half-power beamwidth, peak source temperature, and scan pointing error. The pointing file consists of azimuth, elevation, and accumulated pointing corrections in the xel and el axes. Hereafter, the accumulated pointing corrections are referred to simply as pointing corrections.

During the early period of the measurements described in this article, the boresight program resided in a PC and noise-temperature measurements were entered by an operator. Pointing the antenna was executed from the local control display (LCD). The basic calibration test configuration used is shown in Fig. 2. During 1990–1991, S. R. Stewart of the Ground Antennas and Facilities Engineering Section integrated improved boresight and radiometer system software into a single PC-based module that both controls the radiometer system hardware and directly sends offsets to the antenna servos through the ACS maintainance port. A full (two-axis) boresight now takes approximately 7 min to complete. Further discussion on the boresight methodology and calibration instrumentation may be found in [1,2] and in the DSS 13 BWG antenna Phase 1 Final Report.[1]

IV. Systematic Pointing-Error Modeling

A. Model Generation

Pointing corrections are used to assess performance and also to create or update the systematic pointing-error models. The plot of these numbers versus antenna position is theoretically the error path that the antenna beam would follow if no external corrections at all were loaded into the ACS after each boresight scan. This residual error path then represents just the imperfections of the present error model in use and other antenna boresight corrections resident in the ACS, as well as random error contributions. Its magnitude is thus a measure of the antenna blind-pointing performance. Assuming environmental effects to be minimal and other ACS pointing compensation (e.g., squint, refraction) to be accurate, one may attribute the corrections to the inadequacy of systematic error modeling. The model-building process then proceeds by adding the corrections to those corrections generated by the a priori model used in that particular track. These new values are called total corrections and are used to generate an updated error model.

The Cassegrain-focus systematic pointing-error model for an elevation-over-azimuth mount antenna is shown in Table 1. As shown, the systematic pointing-error list includes such contributors as encoder fixed offsets, azimuth plane tilt, gravitational flexure, and fixed source coordinate errors. A more thorough discussion of the parameters as presented in a 1986 seminar[2] may be found in [3]. PC-based pointing-model software utilized at DSS 13 enables the merging of correction files from multiple star tracks into one total correction file. A second program

[1] M. J. Britcliffe, L. S. Alvarez, D. A. Bathker, P. W. Cramer, T. Y. Otoshi, D. J. Rochblatt, B. L. Seidel, S. D. Slobin, S. R. Stewart, W. Veruttipong, and G. E. Wood, *DSS 13 Beam Waveguide Antenna Project: Phase 1 Final Report*, JPL D-8451 (internal document), Jet Propulsion Laboratory, Pasadena, California, May 15, 1991.

[2] R. L. Riggs, "Antenna Pointing Angle Corrections," DSN Antenna Seminar, Videotapes 49-54 (internal document), Jet Propulsion Laboratory, Pasadena, California, May 1986.

then performs a least-squares fit of the data to any combination of parameters selected from Table 1. The output is a new set of model coefficients (P values in Table 1) that can be manually entered into the ACS. The ACS will then compute pointing corrections from those parameters for any combination of azimuth and elevation. In general, the pointing correction modeling of DSS 13 followed the techniques and guidelines given in the 1986 seminar[3] and in [4].

B. Measurement and Parameter Uncertainties

The modeling process encompasses much analysis and engineering judgment. It involves data archiving and editing correction files from the star tracks. Pointing errors generated by nonsystematic sources such as wind, thermal, refraction, mechanical, and radiometer anomalies must be recognized and edited out as much as possible. The total corrections should be repeatable and uncontaminated by these effects. In the parameter estimation, it is assumed that the pointing data provided by the microwave calibration instrumentation are accurate and measurement uncertainty is small as compared with the magnitude of the data points.

Small calculated pointing errors may be due to random errors in the system noise-temperature measurements rather than actual antenna mispointing. As discussed in [2], the stability of the X-band front-end test package system noise temperature on the ground was very good, with no discernible changes greater than 0.02 K. Depending on the antenna elevation and the strength of the particular radio source being observed, the propagation of 0.01 to 0.1 deg K would result in an uncertainty in the pointing-error estimate of no more than a few tenths of a millidegree. Of greater concern is the on-source temperature measurement uncertainty introduced by the dynamics of the antenna structure and axis servos. In higher than average wind conditions (10–20 mph), the signal jitter (due to mechanical oscillations) observed during measurements on the side of the antenna beam is significantly increased. Through observations of the elevation axis encoder, the mechanical pointing errors in such conditions were seen to approach 2.0 mdeg peak-to-peak (1-sigma). This value is of the same order of magnitude as the preliminary analytical results reported in [5]. To minimize errors incurred in the estimates of the static pointing and efficiency variables (especially at the Ka-band frequency), system temperatures are integrated over a user-specified time interval [2], generally on the order of 3–10 sec. Consistent logging of the weather data enabled the flagging of wind-corrupted pointing corrections.

[3] Ibid.

The quality of a generated model is also dependent on the distribution of the measured beam-pointing errors. The linear dependence of the columns of the measurement-distribution matrix that forms the least-squares problem is strongly dependent on the sky distribution of the observation points [4]. To ensure a satisfactory matrix condition that leads to accurate estimation of all the parameters in Table 1, radio sources at different declinations must be tracked to ensure full ranges of both azimuth and elevation. Various numerical statistics in the modeling program allow assessment of this matrix condition as well as the performance of the parameter fit in terms of estimation residuals.

V. Pointing Calibrations at f1

All the f1 pointing-error modeling was based on X-band tracks. Four iterations of the Cassegrain-focus model were made during the first three months of the f1 calibrations. The final model was obtained during the week of post-holography X-band calibrations, with the antenna main reflector panels in their final adjustment condition. It was based on tracks of the radio sources DR21 and 3C274 (declinations 42.3 and 12.4 deg, respectively). Consecutive tracks on these declinations showed the most repeatability in the pointing, while data from other sources were degraded by high winds (greater than 15 mph) and antenna mechanical malfunctions. The total corrections for each beam axis along with the f1 model predictions are shown in Figs. 3 and 4. The azimuth corrections (which are applied to the azimuth axis servo) are computed from the cross-elevation corrections and are illustrated in Fig. 5. The model coefficients and their theoretical standard deviations derived from the least-squares covariance matrix are shown in Table 2.

The constant declination and hour angle error parameters $P6$ and $P21$ are not included because they were estimated with insignificant magnitude. Only $P2$ was estimated, since the simultaneous estimation of $P1$ and $P2$ resulted in large matrix condition. The elevation corrections imply a negative fixed encoder offset and large residual squint compensation as indicated by $P8$. The different paths for the rising and setting over the tracks shown in Fig. 3 are due to the azimuth dependence of the elevation correction required for the azimuth plane tilt modeled by the $P4$ and $P5$ terms. Theodolite measurements of the DSS 13 azimuth track indicated only a slight plane tilt of 2 mdeg, where, as seen in Table 2, the tilt coefficient is estimated to be almost 8 mdeg. The additional error magnitude was possibly due to an intermittent el-

evation position-encoder error.[4] An apparent motion of the elevation bearing relative to the encoder resulted in a hysteresis-like position-error signature relative to the direction of elevation motion. These errors were sensed as a function of azimuth during the star tracks. Since the f1 calibrations, the magnitude of the problem has apparently been reduced by redesign of the coupling between the antenna structure and the encoder.

Not many data points at azimuths greater than 300 deg were available to use in the modeling. As a result, the model's predictive capability in that region of the sky is degraded, as shown in Figs. 3–5. This also increased the overall standard deviations of the model estimation residuals. They were 2.0 mdeg in xel and 2.6 mdeg in el, resulting in a large root-sum-square standard deviation of 3.3 mdeg.

Figure 6 shows the azimuth–elevation plane trajectories of the star tracks over which the DSS 13 pointing performance will be illustrated. The data points are actual boresight measurement locations. Figure 7 illustrates the beam-pointing corrections resulting from a Ka-band track of 3C274 at f1, whose trajectory is shown in Fig. 6. The measurements were taken in low winds (5–9 mph) and clear skies. The Cassegrain-focus model described above was used during the track. The beam corrections are defined to be the root sum square of the elevation and cross-elevation corrections as computed by the calibration program. As illustrated, the f1 model predicts very well at the high elevations but is degraded at the lower end. Refraction uncertainties at the lower end degraded pointing and systematic error modeling during the entire f1 calibrations. As seen in Fig. 3, very few data points below 20 deg elevation were deemed reliable enough to be incorporated into the measurement distribution. The corrections in Fig. 5 are typical of those sensed during other star tracks at both lower and higher declinations in a favorable environment. The scan-to-scan errors sensed approximately every 10–15 min (obtained by differencing the sequential corrections in Fig. 7) are mostly on the order of 1 mdeg or less. The 3-sigma blind-pointing tolerance of 5.0 mdeg was demonstrated to be met at elevations greater than 17 deg.

VI. Beam-Waveguide Pointing Errors

The calibration of the f3 beam pointing of DSS 13 is unique in that it involves errors contributed by imperfections of the BWG system. Static mirror misalignments and deflections of the mirrors as a function of antenna orientation induce pointing errors that may be sensed at the f3 focus. The pointing calibration approach was to first estimate these errors during the mirror-alignment stage, and then, if possible, try to compensate for them with the existing Cassegrain-focus pointing model.

During the center-fed BWG mirror alignment, center-ray laser theodolite deflection measurements were obtained by M. J. Britcliffe of the Ground Antennas and Facilities Engineering Section. From the antenna pedestal room, a laser at f3 was focused onto a target 100 in. below the antenna hub through all the BWG flat-plate alignment mirrors. The optical measurement configuration is shown in Fig. 8. The antenna was then moved in azimuth and elevation, and the laser focus was sketched on the target. A static misalignment of a mirror or feed in the pedestal room below the antenna track will result in an azimuth-dependent circular trace relative to the mirror set angles of azimuth = 340 deg and elevation = 45 deg. In elevation movement, the deflections of the BWG mirror that is mounted next to the antenna hub (M1 in Fig. 8) cause a change in the alignment of the BWG system and result in pointing errors above and below the 45-deg set angle.

The measured displaced center ray-traces were treated as a translated f1 feed in a Cassegrain antenna, from which crude first-order pointing-error predictions were then computed. This modeling approach ignored any equivalent Cassegrain f1 feed rotations resulting from an angled center ray impinging on the target. The cross-elevation beam errors were estimated to vary as a function of cos (el) and sin (az–340 deg). The expected variation of the elevation errors was with respect to cot (el) and cos (az–340 deg). Constant beam shifts were also expected in each axis. Expanding the sin (az–340 deg) and cos (az–340 deg) terms and reviewing the xel- and el-basis terms in Table 1 indicates that the parameters $P1$, $P2$, $P4$, $P5$, $P6$, $P7$, and $P9$ would accommodate estimation of the new pointing errors introduced by the centerline BWG system. Note that the $P6$ term typically deals with source declination error; however, its functional form aids in accommodating the expected BWG mirror-misalignment effects. The only term in the above expansion not available in the current xel error model is a cos (az) function.

VII. Pointing Calibrations at f3

During the X-band calibrations at f3, the f1 pointing model discussed earlier was used. The residual pointing errors remaining at f1 are shown in Fig. 7 and are then an uncertainty baseline for quantification of the new errors sensed at f3. The f3 pointing corrections in el and xel measured on a 3C84 track (declination 41.5 deg) are

[4] Britcliffe et al., op. cit.

shown versus elevation in Figs. 9 and 10. As indicated, the deflections of the first (and to a lesser extent, second) BWG mirror with elevation change produces beam errors at f3, primarily in the xel axis. An apparent discontinuity in the azimuth bearing rack and encoder gearing interface produces a jump in the cross-elevation corrections at approximately 62 deg azimuth. From the trajectory of source 3C84 shown in Fig. 6, this corresponds to approximately 40 deg elevation for clockwise azimuth travel and 73.5 deg elevation for counterclockwise motion. The former clockwise crossing consistently yielded a larger shift in azimuth (of roughly 9.5 mdeg) and was first observed during the f1 calibrations. A shift in the elevation corrections is also discernible at roughly 41 deg elevation; however, it was not found to be repeatable.

Of the measurement sets obtained during the week of X-band star tracks, only the 3C84 track shown and a full 3C274 track were deemed suitable for calibration purposes. High winds and a malfunctioning subreflector servo positioner contaminated the remainder of the pointing data. The former tracks were added to the f1 pointing-model corrections to yield total antenna corrections. After editing, they were fitted to the parameters $P2$–$P9$, yielding the f3 model presented in Table 3. A comparison of the coefficients above with the f1 model indicates that most of the BWG pointing deflections were picked up by the $P2$ through $P5$ terms and the additional $P6$ term.

There was very little change in the elevation error coefficients. The f3 model fit had residual standard deviations of 2.23 mdeg in xel and 1.91 mdeg in el. These residuals are defined to be the differences between the total el and xel corrections and the computed model predictions for each track, and are shown in Figs. 11 and 12. Both residual signatures in each axis are similar, with the exception of the discontinuities at about 40 deg elevation for the 3C84 track. The residuals also indicate that larger than desirable model uncertainties remain in both axes at the lower elevations, as well as at the meridian crossings.

This model was used in one more X-band track and the subsequent Ka-band calibrations. The el and xel corrections for the 3C123 X-band and two combined 3C84 Ka-band tracks, whose trajectories are illustrated in Fig. 6, are shown in Figs. 13 and 14. These postcalibration measurements were taken in winds less than 10 mph and were typical of the tracks at f3 in a favorable environment. The Ka-band measurements, in general, tended to be more scattered. The pointing-correction signatures remaining for both tracks shown are similar in elevation, thus suggesting no azimuth dependence. They also still resemble the general signature of the source 3C84 elevation corrections needed before the f3 calibration shown in Fig. 9. The cross-elevation residual pointing adjustments in Fig. 14 differ at low elevation and at the meridian crossings. The shifted 3C84 corrections below 40 deg elevation demonstrate the inability of the pointing model in Table 1 to accommodate the large clockwise azimuth discontinuity discussed above. The cause for the divergence of the 3C84 (northern meridian crossing) and 3C123 (southern meridian crossing) corrections in Fig. 14 is still not known.

Beam-pointing corrections computed from the measurements shown in Figs. 13 and 14 are illustrated in Fig. 15. The majority of the scan-to-scan pointing errors sensed for each track are less than or equal to 1.5 mdeg. The larger accumulated beam corrections, which were analyzed in the orthogonal axes above at the higher and lower elevations, were predicted by the f3 pointing-model estimation residuals. Efforts to resolve and compensate for the remaining f3 pointing errors are ongoing and may lead to augmenting the f1 Cassegrain-focus pointing model with extra terms. However, as illustrated in Fig. 15, the model terms shown in Table 1 were capable of meeting the DSS 13 f3 blind-pointing requirement of 5 mdeg at elevations greater than 25 deg.

VIII. Summary and Concluding Remarks

The methods employed and the final results obtained for the initial pointing calibrations of the DSS 13 BWG antenna from July 1990 through January 1991 have been presented. The primary objective for this first phase of the DSS 13 antenna project was to meet a 5.0-mdeg blind-pointing specification under low (less than 10 mph) wind conditions at both the f1 and f3 focal points. Pointing measurements (made simultaneously with efficiency measurements) demonstrated that this goal was achieved over a wide range of azimuths and at elevations greater than 17 deg at f1 and greater than 25 deg at f3. It was also shown that the current Cassegrain-focus systematic pointing-error model residing in the DSS 13 ACS was able to accommodate the pointing degradations introduced by the centerline BWG, at least to the level of accuracy required for the initial performance testing.

The DSS 13 antenna pointing calibration effort presented in this article is preliminary. A more thorough analytical modeling effort of the center-fed BWG system pointing corrections needs to be pursued. Repeatability of the remaining pointing correction residuals at f3 offers encouragement that further predictive performance may be achievable by augmenting the Cassegrain-focus systematic error model with new terms. With respect to station ca-

pabilities, the pointing will have to be continuously monitored and recalibrated through the many mechanical and microwave upgrades and experiments planned for this research and development antenna. For example, the beam pointing was observed to have shifted 30 mdeg in January 1991 after minor optical realignment of the ellipsoidal BWG mirror in the pedestal room. All the pointing-model software used in the preliminary calibrations is now resident at DSS 13. However, further training of DSS 13 personnel is recommended to ensure maintenance of the initial levels of accuracies achieved.

The characterization of pointing performance in higher wind conditions and at the lower elevation angles is still incomplete. On windy days (greater than 15 mph), it was observed that the DSS 13 beam pointing (measured roughly every 10 min) does not yet meet the 5.0-mdeg 3-sigma blind-pointing goal. The dynamic pointing errors, as sensed through the apparent noise-temperature jitter, were a problem at Ka-band and necessitated larger radiometer integration time intervals. More pointing measurements need to be taken in conjunction with the analytical investigations initiated in [5] in order to study and credibly quantify these wind-induced performance degradations. Likewise, more star tracking at the lower elevations is needed to classify the low-elevation pointing errors in terms of refraction uncertainty and/or mechanical deficiencies in the pointing model. The option for real-time surface weather inputs to the ACS refraction model is not yet implemented. This utility needs to be thoroughly tested and its performance measured against the default refraction model resident in the DSS 13 ACS.

Acknowledgments

The author thanks R. L. Riggs for the development of the boresighting program and pointing-model software used during the testing period discussed here. A team effort including M. J. Britcliffe, M. M. Franco, T. Y. Otoshi, S. D. Slobin, and S. R. Stewart provided the pointing and efficiency measurements. H. Ahlstrom provided many helpful discussions on the DSS 13 ACA, and M. J. Britcliffe provided the theodolite measurements necessary for the BWG pointing-error modeling. Lastly, the Goldstone DSS 13 personnel are gratefully acknowledged for their support throughout the entire performance-testing program.

References

[1] S. D. Slobin, "Efficiency Calibration of the DSS 13 34-Meter Diameter Beam Waveguide Antenna at 8.45 and 32 GHz," *TDA Progress Report 42-106* (this issue), vol. April–June 1991, Jet Propulsion Laboratory, Pasadena, California, pp. 283–297, August 15, 1991.

[2] T. Y. Otoshi, S. R. Stewart, and M. M. Franco,"A Portable X-band Front-End Test Package for Beam-Waveguide Antenna Performance Evaluation, Part I: Design and Ground Tests," *TDA Progress Report 42-103*, vol. July–September, 1990, Jet Propulsion Laboratory, Pasadena, California, pp. 135–150, November 15, 1990.

[3] C. N. Guiar, F. L. Lansing, and R. Riggs, "Antenna Pointing Systematic Error Model Derivations," *TDA Progress Report 42-88*, vol. October–December 1986, Jet Propulsion Laboratory, Pasadena, California, pp. 36–46, February 15, 1987.

[4] L. S. Alvarez, "An Analysis of the Least Squares Problem for the DSN Systematic Pointing Error Model," *TDA Progress Report 42-104*, vol. October–December 1990, Jet Propulsion Laboratory, Pasadena, California, pp. 17–29, February 15, 1991.

[5] W. Gawronski and J. A. Mellstrom, "Modeling and Simulations of the DSS 13 Antenna Control System," *TDA Progress Report 42-106* (this issue), vol. April–June 1991, Jet Propulsion Laboratory, Pasadena, California, pp. 205–248, August 15, 1991.

Table 1. Systematic pointing error sources and model terms

Error source	Model function	
	Cross-elevation error	Elevation error
Az[a] collimation	P_1 [d]	–
Az encoder fixed offset	P_2 cos (el)	–
Az/el skew	P_3 sin (el)	–
Az axis tilt	P_4 sin (el) cos (az)	$-P_4$ sin (az)
Az axis tilt	P_5 sin (el) sin (az)	P_5 cos (az)
Source dec[b]	P_6 sin (az)	P_6 sin (el) cos (az)
El[c] encoder fixed offset	–	P_7
Gravitational flexure	–	P_8 cos (el)
Residual refraction	–	P_9 cot (el)
Source HA[e]	P_{21} cos (dec)	–

[a] Az refers to azimuth angle.
[b] Dec refers to declination angle.
[c] El refers to elevation angle.
[d] P refers to parameter value.
[e] HA refers to hour angle.

Table 2. f1 systematic pointing-error model coefficients

Coefficient	Value, mdeg	Standard deviation, mdeg
$P2$	4.23	0.27
$P3$	10.85	0.22
$P4$	−7.70	0.12
$P5$	0.52	0.14
$P7$	−22.93	0.32
$P8$	−44.37	0.87
$P9$	−4.53	0.25

Table 3. f1 systematic pointing-error model coefficients

Coefficient	Value, mdeg	Standard deviation, mdeg
$P2$	16.23	0.36
$P3$	−5.36	0.27
$P4$	−9.43	0.15
$P5$	5.62	0.53
$P6$	−5.12	0.46
$P7$	−22.14	0.39
$P8$	−46.73	1.01
$P9$	−5.31	0.28

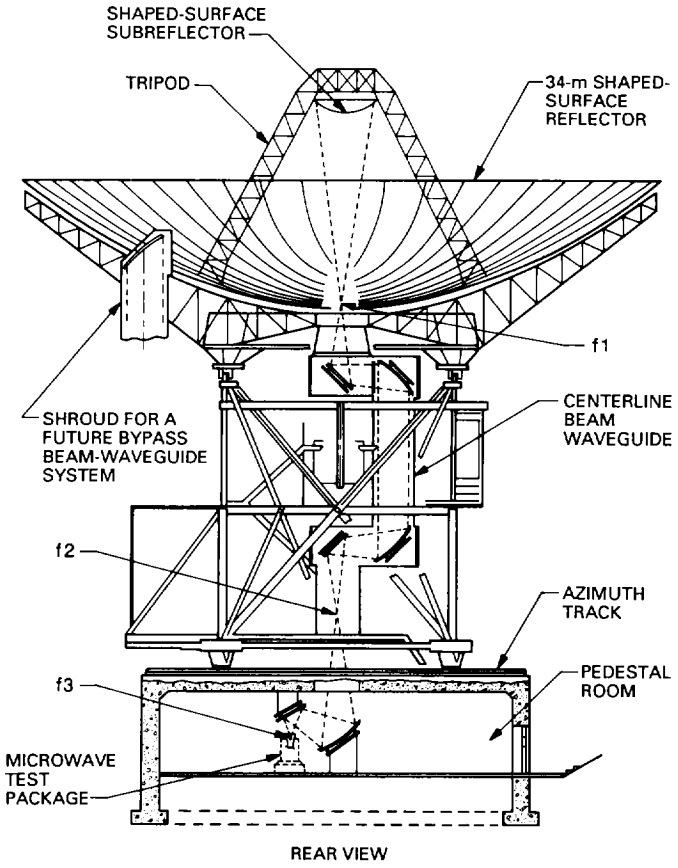

Fig. 1. Outline drawing of DSS 13 antenna.

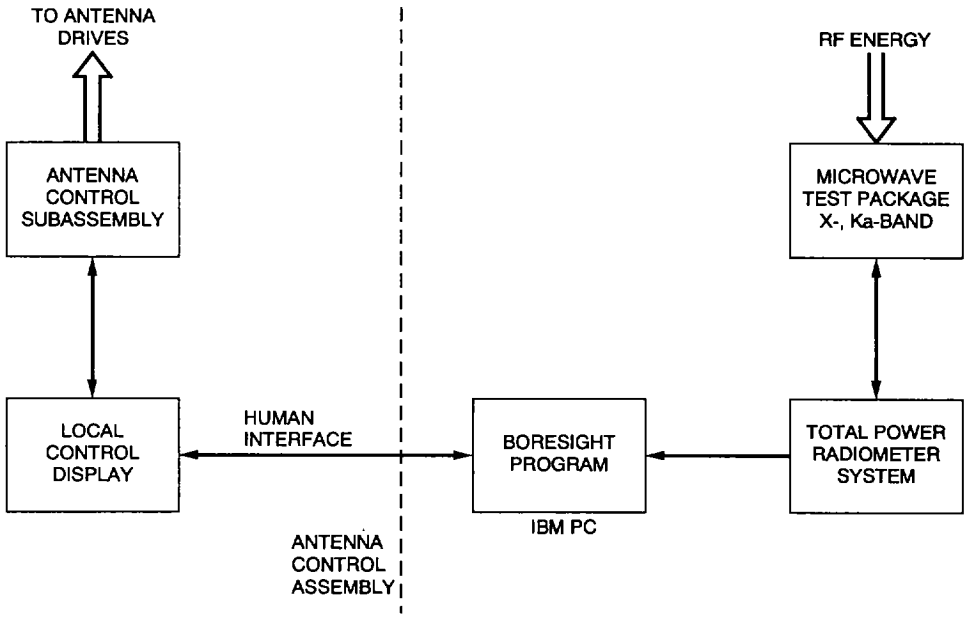

Fig. 2. Calibration instrumentation configuration.

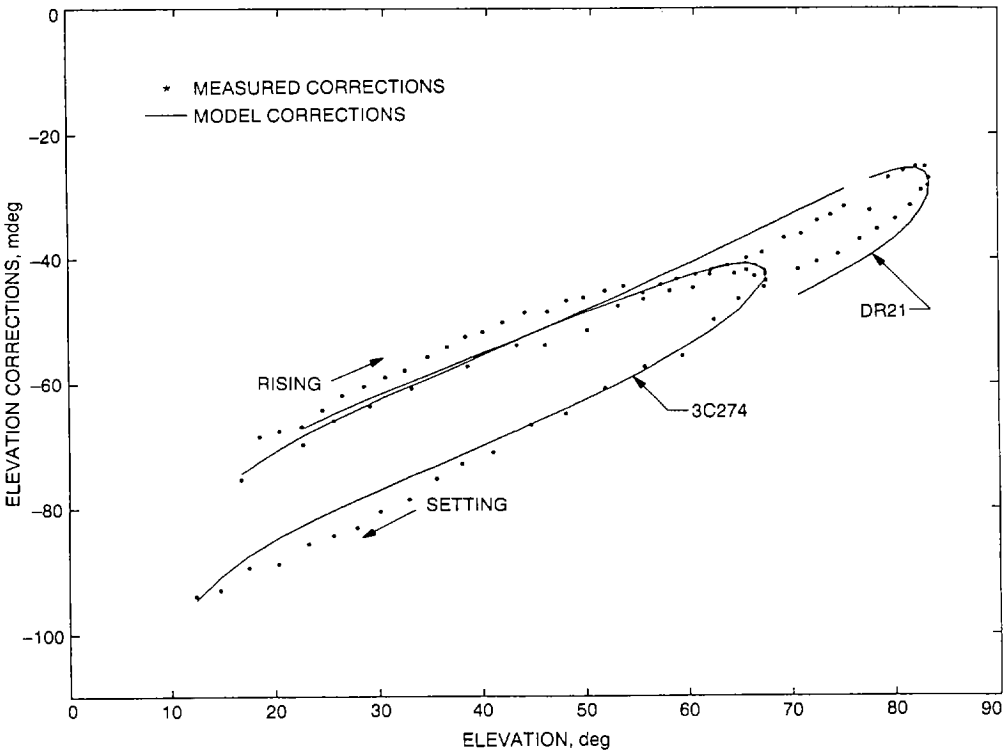

Fig. 3. f1 total elevation corrections versus f1 model predictions.

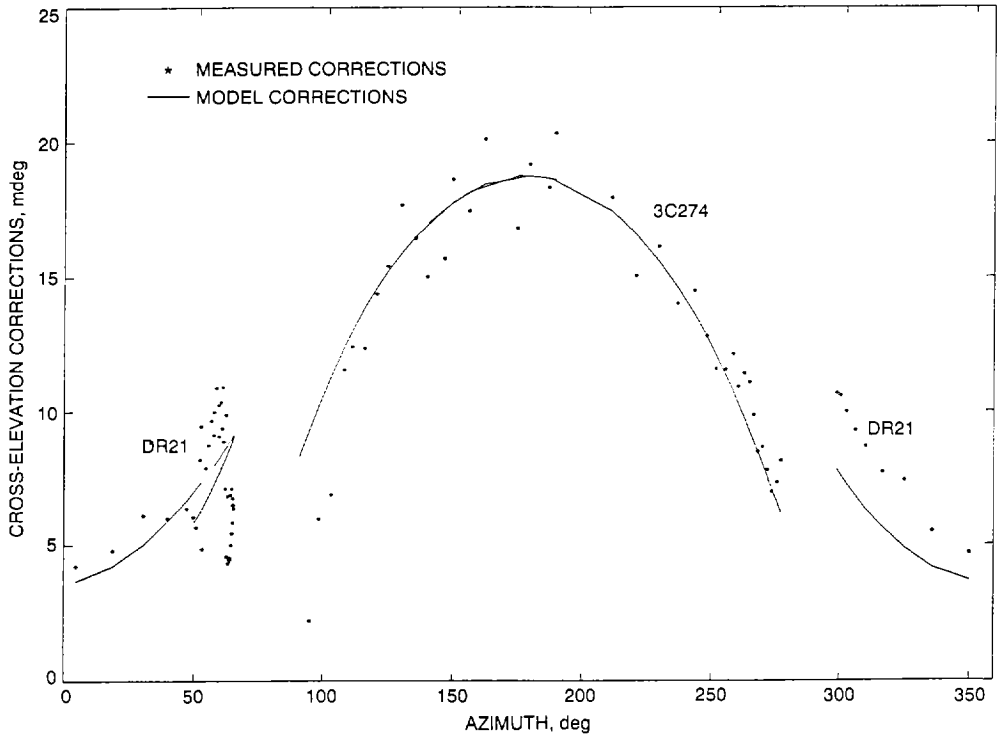

Fig. 4. f1 total cross-elevation corrections versus f1 model predictions.

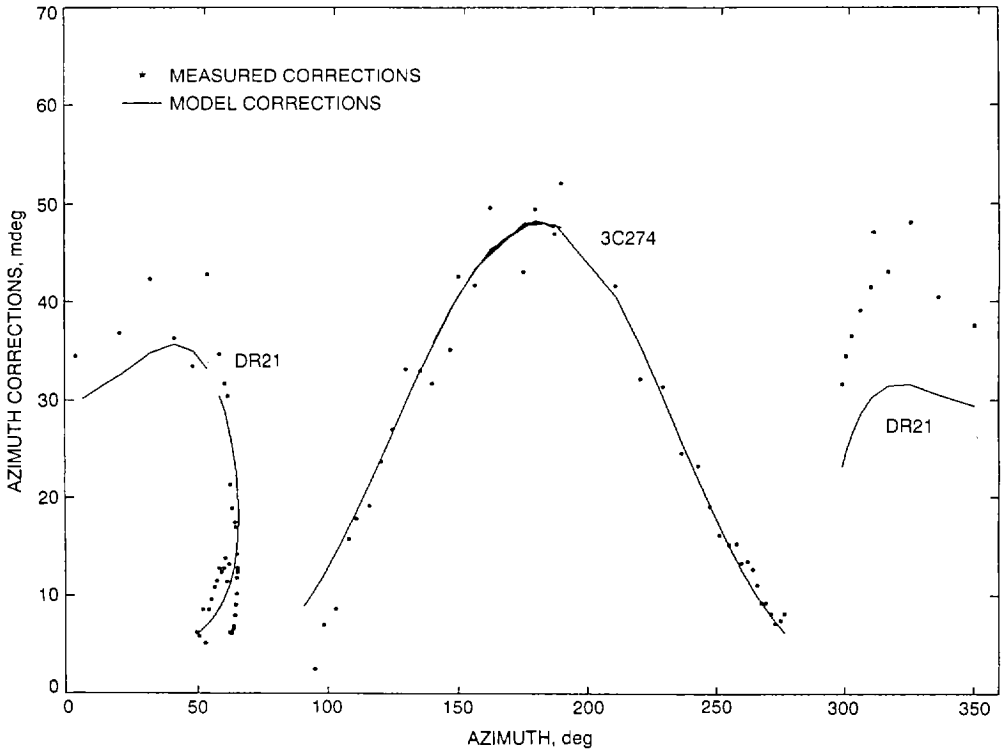

Fig. 5. f1 total azimuth corrections versus f1 model predictions.

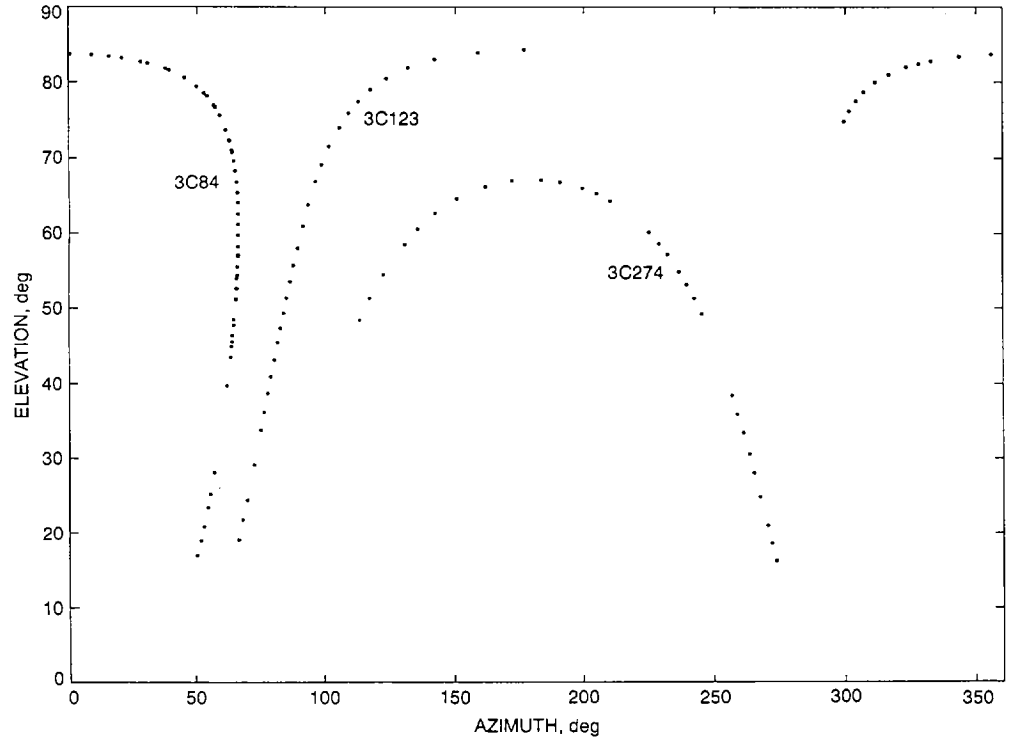

Fig. 6. Radio source trajectories for DSS 13 pointing performance assessment.

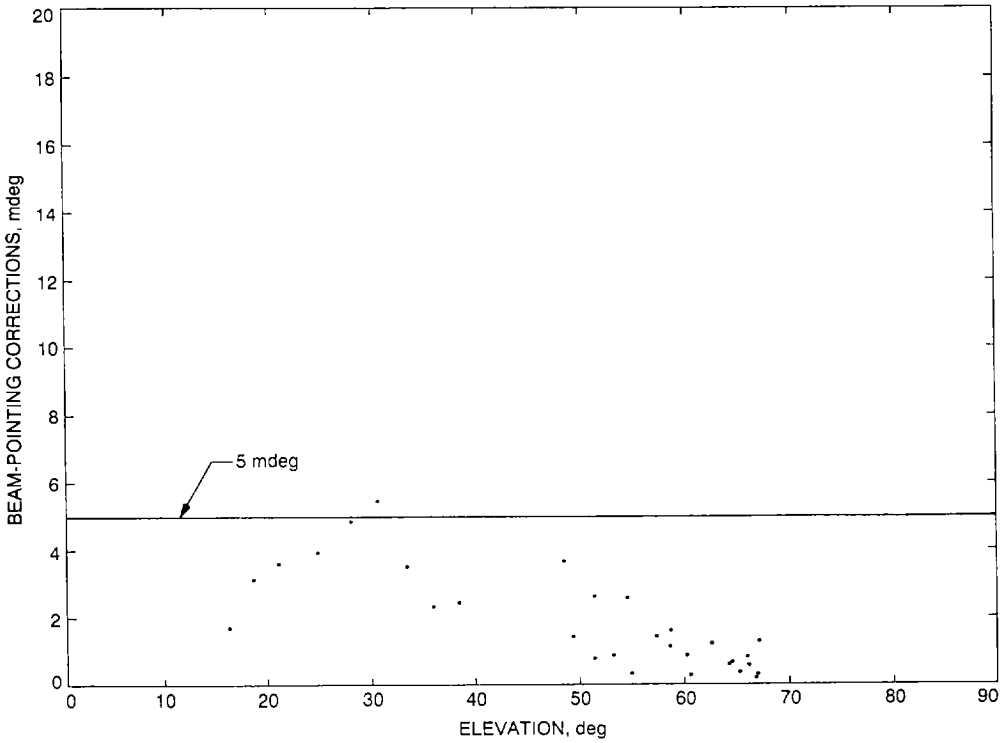

Fig. 7. Beam-pointing corrections for 3C274 track, DOY 288, 1990, Ka-band at f1.

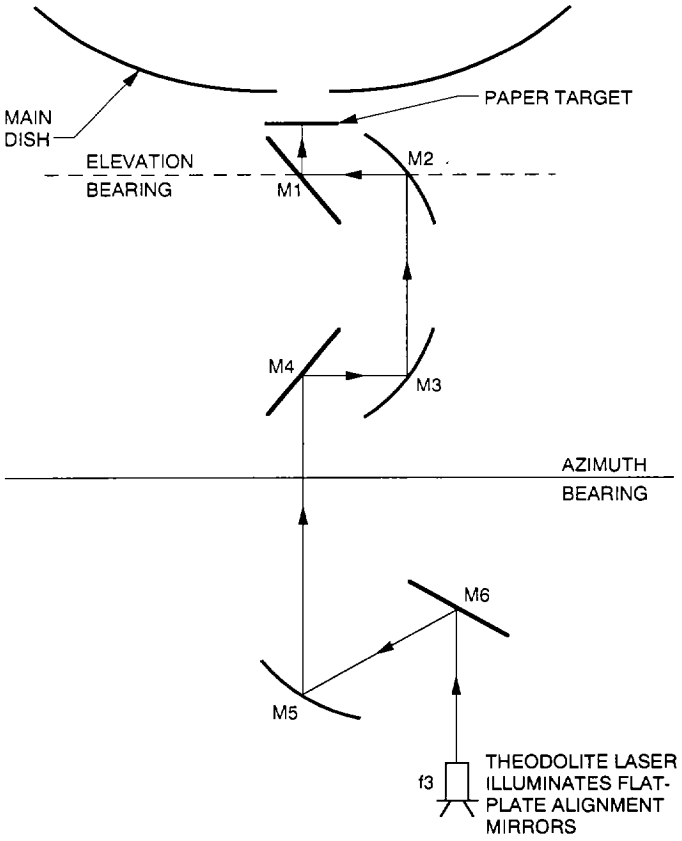

Fig. 8. Theodolite laser experiment configuration.

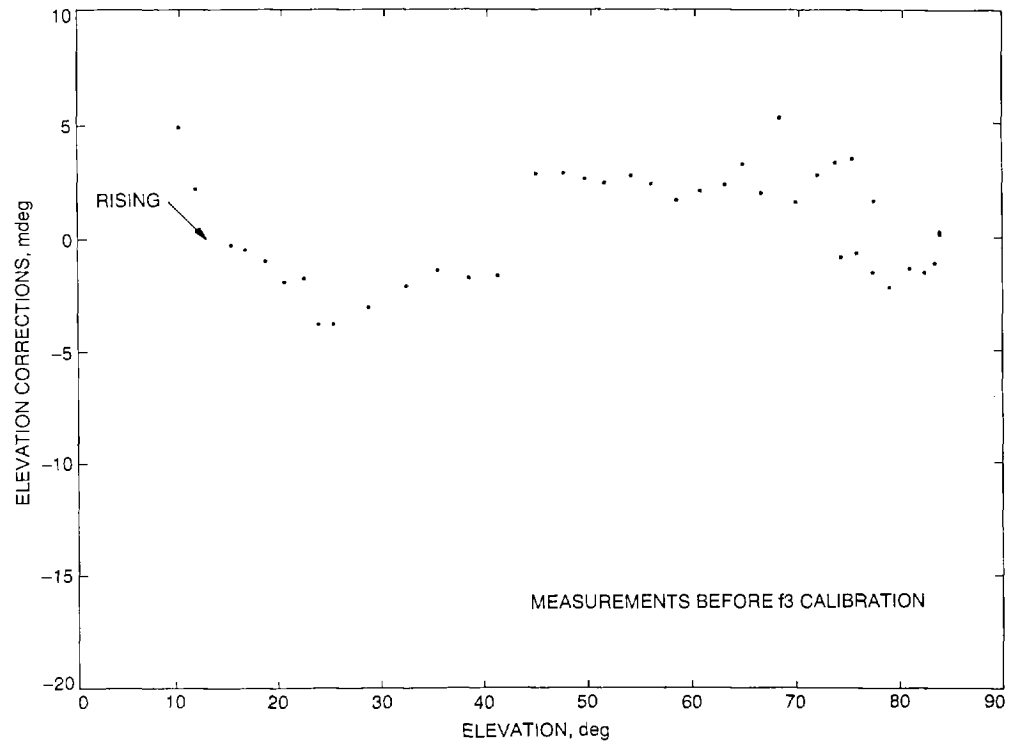

Fig. 9. Elevation pointing corrections for 3C84 track, DOY 311, 1990, X-band at f3.

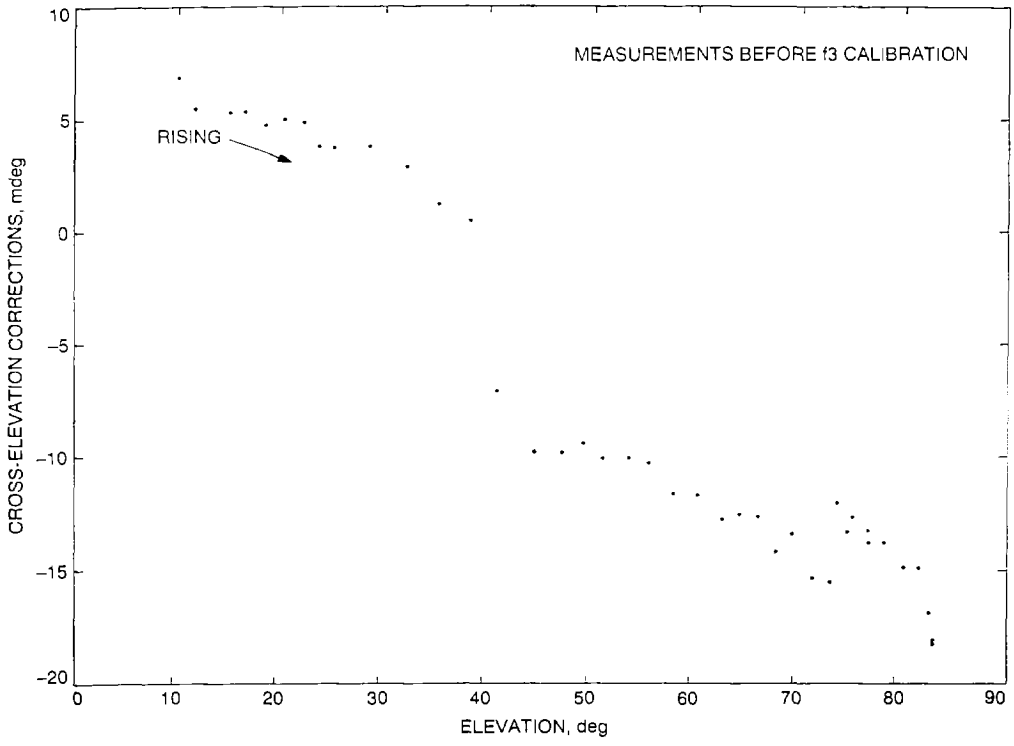

Fig. 10. Cross-elevation pointing corrections for 3C84 track, DOY 311, 1990, X-band at f3.

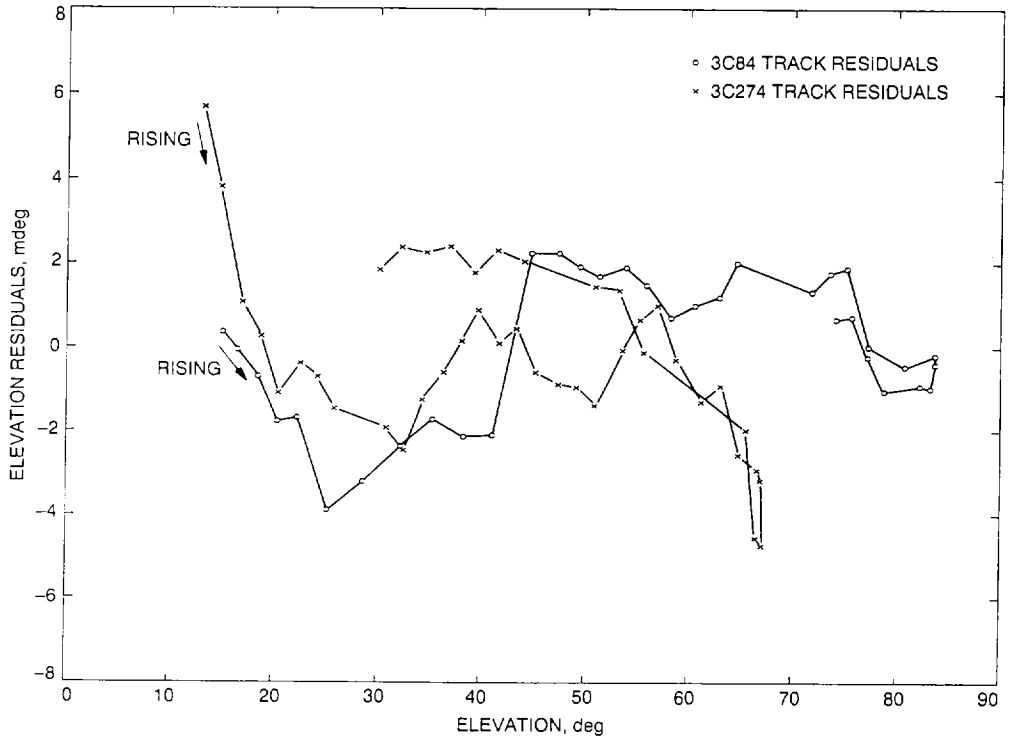

Fig. 11. f3 pointing model elevation residuals.

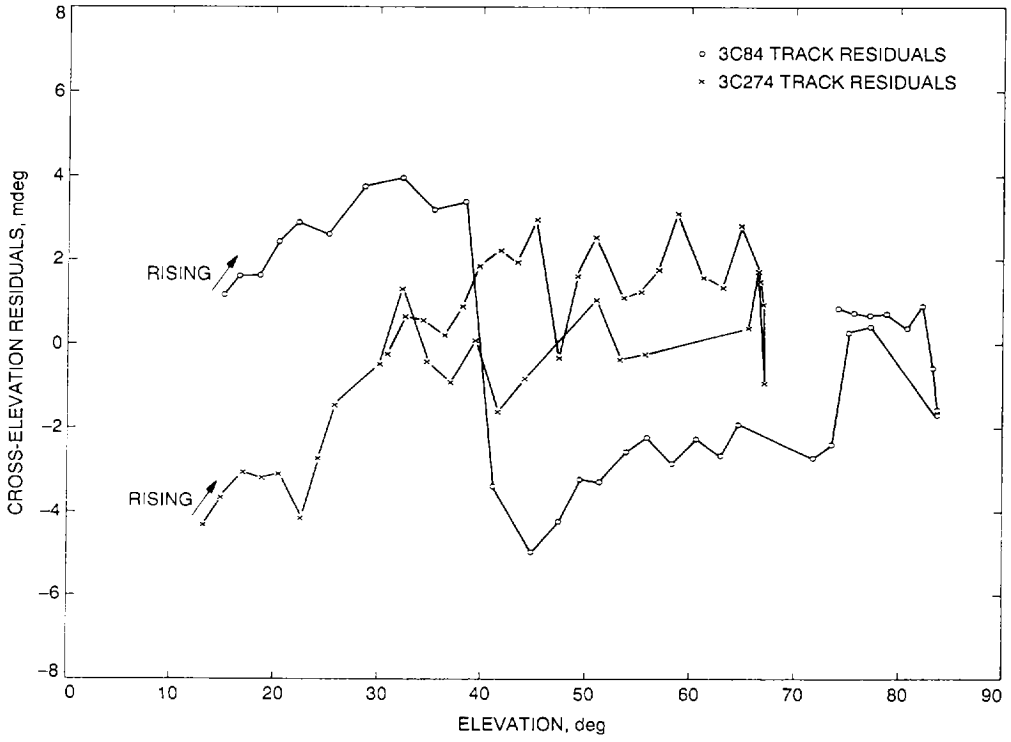

Fig. 12. f3 pointing model cross-elevation residuals.

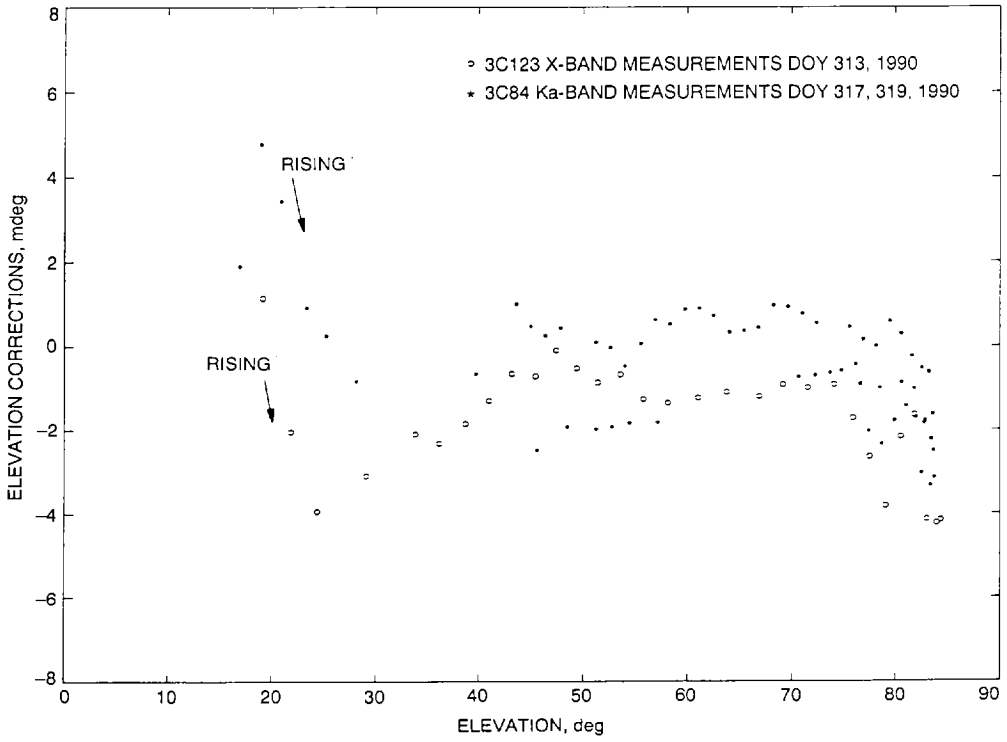

Fig. 13. Elevation pointing corrections for 3C123 and 3C84 tracks at f3.

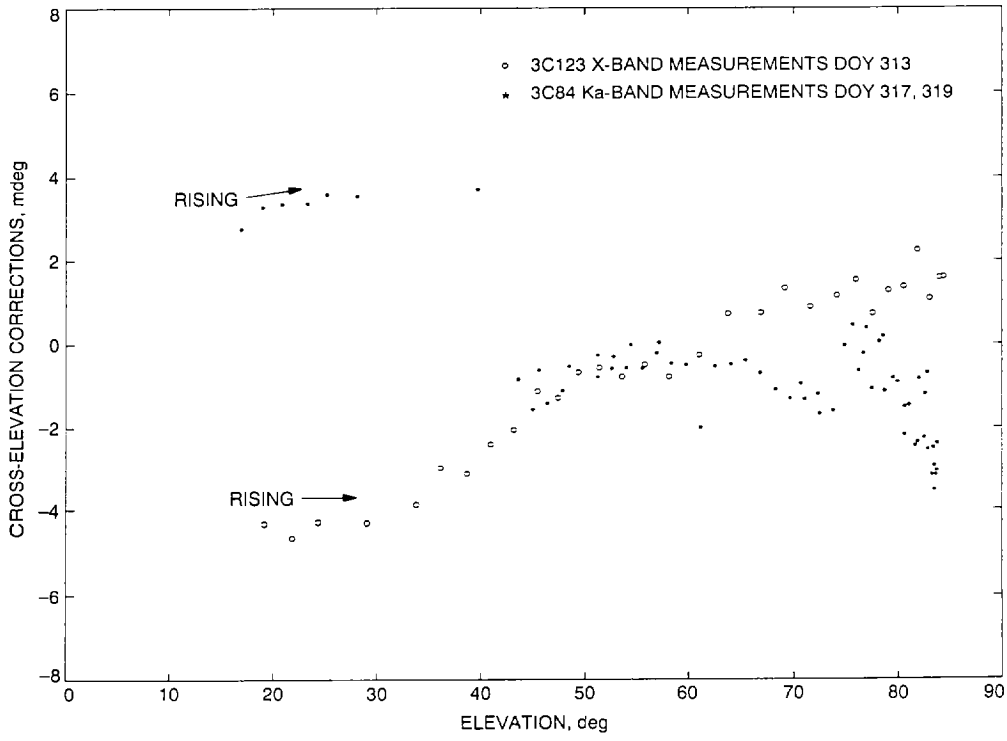

Fig. 14. Cross-elevation corrections for 3C123 and 3C84 tracks at f3.

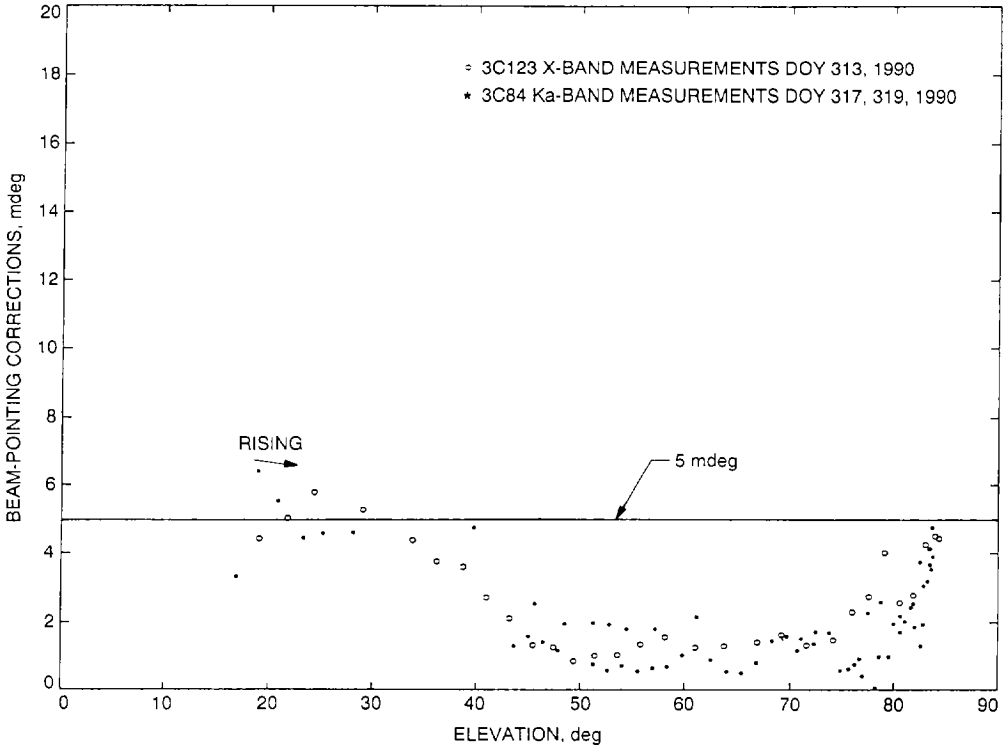

Fig. 15. Beam-pointing corrections for 3C123 and 3C84 tracks at f3.